VIP Cofactors

DOI: 10.1002/anie.201102724

Spectroscopic Characterization of the Isolated Iron–Molybdenum Cofactor (FeMoco) Precursor from the Protein NifEN**

Aaron W. Fay, Michael A. Blank, Chi Chung Lee, Yilin Hu, Keith O. Hodgson,* Britt Hedman,* and Markus W. Ribbe**

Nitrogenase provides the biochemical machinery for the conversion of atmospheric dinitrogen (N_2) into bioavailable ammonia (NH_3). The best-characterized molybdenum (Mo)-nitrogenase consists of two redox-active metalloproteins: the iron (Fe) protein and the molybdenum–iron (MoFe) protein.[1] During catalysis, the Fe protein mediates the transfer of electrons to the iron–molybdenum cofactor (FeMoco) site of the MoFe protein, where substrate reduction eventually occurs. FeMoco ([$MoFe_7S_9X$-homocitrate], X = C, N or O) is arguably the most complex metallocluster found in nature, and the biosynthesis of this cofactor is an intricate process that involves the participation of many protein factors.[2] NifEN is one of the key players in this process. An $\alpha_2\beta_2$-tetrameric protein that is highly homologous to the MoFe protein in primary sequence and cluster type, NifEN serves as a scaffold for the maturation of a FeMoco precursor into a fully assembled cofactor prior to its transfer to the target location within the MoFe protein.[2] Apart from playing a crucial role in cofactor biosynthesis, NifEN is also a catalytic homologue of MoFe protein that is capable of reducing acetylene (C_2H_2) and azide (N_3^-), the alternative substrates of nitrogenase.[3]

Two forms of NifEN have been characterized (see Table S1 for designations of proteins used in this work). One, designated NifEN, contains two cluster species: a [Fe_4S_4] cluster at each α/β subunit interface and a FeMoco precursor within each α subunit.[4] The other, designated Δ*nifB* NifEN, only contains the [Fe_4S_4] cluster, as the protein is expressed in a genetic background where *nifB*—the gene encoding an indispensable factor for FeMoco synthesis—is deleted.[4] The difference between the cluster compositions of the two NifEN species has permitted the elucidation of the EXAFS-based structure of precursor by subtracting the spectrum of Δ*nifB* NifEN from that of NifEN, and the derivation of a Mo/homocitrate-free precursor structure that closely resembles the Fe/S core of the mature cofactor provides significant insights into the biosynthetic mechanism of FeMoco.[5] On the other hand, the mixed cluster composition of NifEN has hampered the direct examination of the physiochemical properties of the precursor without the interference of the [Fe_4S_4] cluster. Herein, we report the first isolation of the FeMoco precursor from NifEN, the EPR and activity analyses of the precursor in the isolated- and reconstituted-states, and the XAS/EXAFS investigation of the electronic structure of this isolated cluster.

Using a previously established acid-treatment procedure,[6] the FeMoco precursor was extracted from NifEN into *N*-methylformamide (NMF) at a yield of 62% and a purity of 96%. In the dithionite-reduced state, the isolated precursor exhibits a near-axial $S = 1/2$ EPR signal at $g = 1.97$ (Figure 1a, experiment 1). This signal is clearly distinct from the rhombic $S = 1/2$ signal that originates from the permanent [Fe_4S_4] clusters in Δ*nifB* NifEN, which exhibit g values at 2.07, 1.95, and 1.90 (Figure 1a, experiment 2). Nevertheless, upon the incorporation of the precursor into Δ*nifB* NifEN, the two cluster species of the reconstituted NifEN give rise to a composite $S = 1/2$ signal at $g = 2.09$, 1.95, and 1.88 (Figure 1a, experiment 3), which is indistinguishable from that displayed by NifEN (Figure 1a, experiment 4). This result is consistent with our earlier observation that NifEN contains two $S = 1/2$ species with different temperature- and power-dependent behaviors;[4] moreover, it suggests that an intact form of precursor has been extracted into NMF, which is competent in reconstituting Δ*nifB* NifEN. It should be noted, however, that the percentage of precursor incorporation is approximately 67% based on the quantification of the precursor-specific $S = 1/2$ signal.[7] Such an incomplete precursor incorporation could be explained by the inhibitory effect of NMF on the reconstitution process, a phenomenon documented earlier for the reconstitution of Δ*nifB* MoFe protein by NMF-extracted FeMoco.[6]

In the IDS (indigo disulfonate)-oxidized state the isolated precursor displays a distinct EPR feature at $g = 1.93$ (Figure 1b, experiment 1), which could arise from an $S = 1/2$ state. This feature is absent from the spectrum of the precursor-

[*] A. W. Fay,[+] C. C. Lee, Dr. Y. Hu, Prof. M. W. Ribbe
Department of Molecular Biology and Biochemistry
University of California, Irvine
Irvine, CA 92697 (USA)
E-mail: yilinh@uci.edu
mribbe@uci.edu
M. A. Blank,[+] Prof. K. O. Hodgson
Department of Chemistry, Stanford University
Stanford, CA 94305 (USA)
E-mail: hodgson@ssrl.slac.stanford.edu
Prof. K. O. Hodgson, Prof. B. Hedman
Stanford Synchrotron Radiation Lightsource, SLAC
Stanford University
Menlo Park, CA 94025 (USA)
E-mail: hedman@ssrl.slac.stanford.edu
[+] These authors contributed equally to this work.

[**] This work was supported by Herman Frasch Foundation Grant 617-HF07 (M.W.R.), NIH Grant GM 67626 (M.W.R.), and NIH Grant RR 01209 (K.O.H.). SSRL operations are funded by the DOE BES, and the SSRL Structural Molecular Biology Program by NIH NCRR BTP and DOE BER.

Supporting information for this article is available on the WWW under http://dx.doi.org/10.1002/anie.201102724.

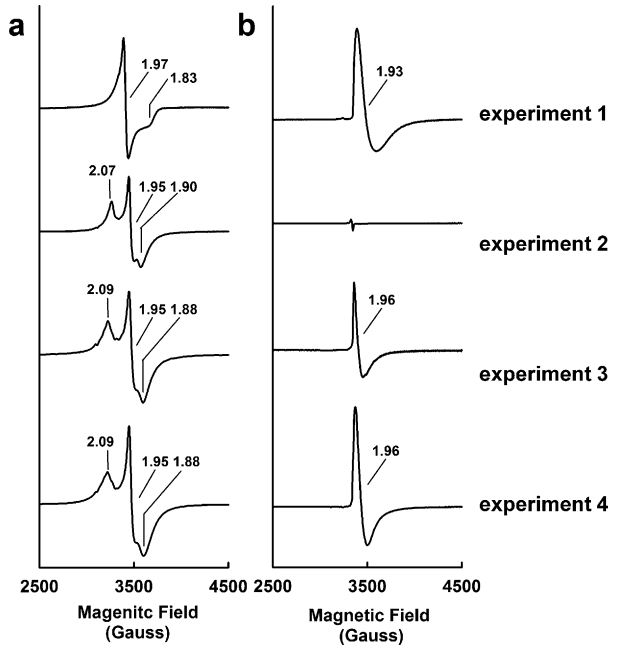

Figure 1. EPR properties of isolated FeMoco precursor (experiment 1), Δ*nifB* NifEN (experiment 2), FeMoco precursor-reconstituted Δ*nifB* NifEN (experiment 3), and NifEN (experiment 4) in a) dithionite-reduced and b) IDS-oxidized states. The dithionite-reduced samples were measured at 10 K, whereas the IDS-oxidized samples were measured at 15 K. All protein concentrations were 30 mg mL^{-1}. The *g* values are indicated.

deficient Δ*nifB* NifEN (Figure 1 b, experiment 2); however, it can be recovered upon the incorporation of precursor into Δ*nifB* NifEN, with a somewhat sharpened line-shape and a slightly shifted *g* value of 1.96 (Figure 1 b, experiment 3). The minor changes of this signal reflect the impact of protein environment on the precursor. More importantly, the same $g = 1.96$ signal can be observed in the spectrum of IDS-oxidized NifEN (Figure 1 b, experiment 4), again demonstrating the successful reconstitution of Δ*nifB* NifEN by the isolated precursor. Compared to the signal in NifEN, the reconstituted signal is approximately 56% in magnitude, which is consistent with the percentage of precursor incorporation (see above).

The biochemical properties of the precursor were subsequently examined by comparing the activities of the precursor-reconstituted Δ*nifB* NifEN (designated NifEN*) with those of NifEN in the in vitro assays of cofactor maturation (Table 1) and substrate reduction (Table 2). In the case of the former, the NifEN- associated precursor was first converted into a mature FeMoco and then used as a FeMoco source to activate the cofactor-deficient Δ*nifB* MoFe protein;[8] whereas in the case of the latter, NifEN was analyzed for its capacity as a catalytic homologue of MoFe protein in C_2H_2- and N_3^--reduction.[3] Compared to NifEN, NifEN* exhibits 64–70% activity in the cofactor maturation assays (Table 1) and 58–60% activity in the substrate reduction assays (Table 2). Thus, the relative activity of NifEN* to NifEN (58–70%) is consistent with the percentage of precursor incorporation (56–67%, see above), suggesting

Table 1: FeMoco maturation activities of as-isolated NifEN and reconstituted NifEN*.

Species	Substrate	Product (nmol mg^{-1} protein/min)[a]		
		NH_3	H_2	C_2H_4
NifEN	C_2H_2/Ar	–	–	795 ± 57 (100)
	H^+/Ar	–	1007 ± 87 (100)	–
	N_2	332 ± 41 (100)	185 ± 8 (100)	–
NifEN*	C_2H_2/Ar	–	–	509 ± 21 (64)
	H^+/Ar	–	707 ± 33 (70)	–
	N_2	233 ± 27 (70)	125 ± 10 (68)	–

[a] Activities of NifEN are set as 100%, and percentages of activities of NifEN* relative to those of NifEN are given in parentheses.

Table 2: Substrate reducing activities of as-isolated NifEN and reconstituted NifEN*.

Species	Substrate	Product (nmol mg^{-1} protein/min)[a]	
		NH_3	C_2H_4
NifEN	C_2H_2/Ar	–	53 ± 2 (100)
	N_3^-/Ar	65 ± 6 (100)	–
NifEN*	C_2H_2/Ar	–	31 ± 2 (58)
	N_3^-/Ar	39 ± 4 (60)	–

[a] Activities of NifEN are set as 100%, and percentages of the activities of NifEN* relative to those of NifEN are given in parentheses.

that the isolated precursor is fully proficient in both biosynthesis and catalysis.

Interestingly, the isolated precursor is also capable of directly activating Δ*nifB* MoFe protein, a cofactor-deficient structural homologue to NifEN (Table 3).[9] However, the

Table 3: Activation of Δ*nifB* MoFe protein by FeMoco and precursor.

Cluster	Substrate	Product (nmol mg^{-1} protein/min)[a]		
		NH_3	H_2	C_2H_4
FeMoco	C_2H_2/Ar[b]	–	84 ± 5 (83)	1187 ± 18 (96)
	H^+/Ar	–	1362 ± 57 (88)	–
	N_2	618 ± 52 (92)	254 ± 17 (98)	–
Precursor	C_2H_2/Ar[b]	–	371 ± 29 (9)	119 ± 6 (10)
	H^+/Ar	–	474 ± 22 (6)	–
	N_2	0 (N/A)[c]	459 ± 36 (5)	–

[a] Percentages of activities retained after subjecting the samples to the gel filtration chromatography are given in parentheses. [b] Maximum activity was observed at 10% and 60% C_2H_2, respectively, for the activation of Δ*nifB* MoFe protein by FeMoco and precursor. [c] N/A = not applicable.

catalytic profile of the precursor-activated Δ*nifB* MoFe protein differs drastically from that of the FeMoco-reconstituted Δ*nifB* MoFe protein. Most notably, the precursor-activated Δ*nifB* MoFe protein is unable to reduce N_2 to NH_3; whereas its ability to evolve H_2 in the presence of N_2 is 1.8-fold higher than the FeMoco-reconstituted Δ*nifB* MoFe protein (Table 3). Similarly, the ability of the precursor-activated Δ*nifB* MoFe protein to reduce C_2H_2 to C_2H_4 is only 10% relative to that of the FeMoco-reconstituted Δ*nifB* MoFe protein, yet its ability to evolve H_2 in the presence of C_2H_2 is 4.3-fold higher than that of the FeMoco-reconstituted

Δ*nifB* MoFe protein (Table 3). Clearly, there is a shift toward the H_2 evolution in the case of the precursor-activated Δ*nifB* MoFe protein. Such a disproportionately altered substrate-reducing profile suggests that the precursor is not properly inserted into the Δ*nifB* MoFe protein. Consistent with this hypothesis, the activity of the precursor/Δ*nifB* MoFe protein mixture is nearly abolished (5–10% of the initial activity) once it is passed through a gel filtration chromatography column; whereas the activity of the FeMoco/Δ*nifB* MoFe protein mixture is largely unaffected (83–98% of the original activity) following the same treatment (Table 3). Apparently, the precursor is only loosely associated with the Δ*nifB* MoFe protein and, therefore, easily separable from the protein. This observation is consistent with our previous report that homocitrate—a component that is absent from the precursor composition—plays an essential role in properly incorporating the cofactor into the MoFe protein.[10]

The electronic structure of the isolated precursor was further investigated by X-ray absorption spectroscopy (XAS) analysis. The isolated precursor displays an overall edge structure that is typical of an iron–sulfur cluster; moreover, it shows a 1s→3d pre-edge transition feature in the iron K-edge XAS spectrum that is remarkably similar in shape and intensity to that of the mature cofactor (Figure 2a). Comparison between the second derivatives of this region reveals nearly identical pre-edge shape and peak location in the respective spectrum of isolated precursor and FeMoco, with a subtle shift to lower energy (0.4 eV) in the first pre-edge transition and slight variations of intensities in the 7120–7125 eV region of the precursor spectrum (Figure 2b), further illustrating a high degree of conservation between the two clusters in average iron geometry. The EXAFS data of the isolated precursor (Figure 2c) were best modeled by an eight-iron cluster, with distances (Table 4) in good agreement with the fit values of data collected on the NifEN-bound precursor of *Azotobacter vinelandii*[5] but in contrast to those from a study of a similar *Klebsiella pneumoniae* system.[11] The most substantial constituents of the fit are 3 sulfur atoms at 2.26 Å and a split iron shell with a short path at 2.65 Å and a long path at 2.85 Å, respectively. Additionally, it was necessary to include a long, cross-cluster, iron–iron path at 3.71 Å with a coordination number of 1.5 in order to fit the distant intensity peak in the Fourier transform (Figure 2d). The inclusion of this path generated a very significant improvement to the goodness of fit, suggesting that a well-structured cluster was extracted intact from the protein. Collectively, the fits to the data of the isolated precursor are consistent with an eight-iron homologue of FeMoco, in which the terminal molybdenum atom in the native cofactor—along with homocitrate—is replaced by an iron atom (Figure 3).

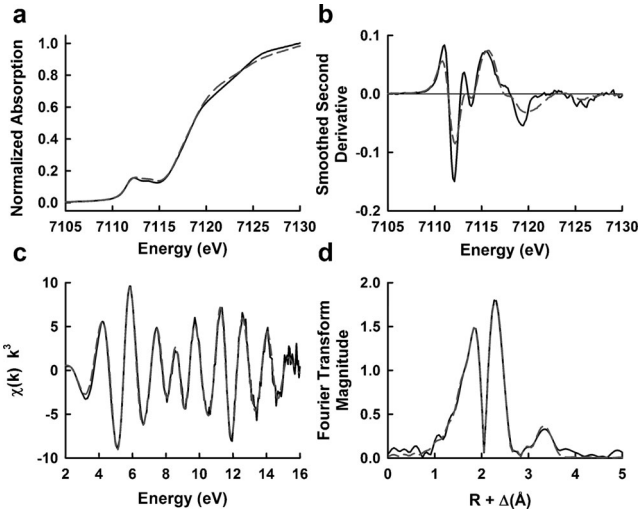

Figure 2. Iron K-edge XAS of a) NMF-isolated FeMoco (solid black line) and iron-only NifEN precursor (dashed dark gray line) and b) smoothed second derivatives; c) k^3-weighted iron K-edge EXAFS of iron-only NifEN precursor (solid black line) overlaid with the best fit represented in Table 4 (dashed dark gray line) and d) the Fourier transforms thereof.

Table 4: Best fits for the Fe K-edge EXAFS data of isolated precursor over the *k*-range of 2–16 $Å^{-1}$.[a]

Scatterer	Isolated precursor (from NifEN)		
	N	*R* [Å]	σ [$Å^2$]
Fe–X	0.7	1.99	0.0039
Fe–S	3.0	2.26	0.0038
Fe–Fe short	3.3	2.65	0.0046
Fe–Fe short	0.5	2.85	0.0074
Fe–Fe long	1.5	3.71	0.0046
ΔE_0 [eV]		−10.8	
Weighted F		0.141	

[a] Coordination number (*N*), interatomic distance (*R*, Å), mean-square thermal and static disorder in distance (σ^2, $Å^2$), and EXAFS threshold energy adjustment from 7130 eV (ΔE_0, eV) were varied in the fits. Estimated errors are ±0.02 Å in *R*, ±0.0001 $Å^2$ in σ^2, and ±20% in N. The goodness of fit, *F*, is defined as $F=[\Sigma k^6(\chi_{exper.}-\chi_{calcd})^2/\Sigma k^6(\chi_{exper.})^2]^{0.5}$. The Fe-X distance was calculated by assuming X as *N*, although indistinguishable results could be obtained by assuming X as C or O.

In addition to the final best fit itself, the process of fitting disclosed two distinct patterns that offered further support to an eight-iron structure of the isolated precursor. First, the goodness of fit always improved with the reduction of the coordination number of the 3.7 Å iron paths. In an eight-iron model, only the six central iron atoms "see" two iron scattering paths at 3.7 Å, whereas the two terminal iron atoms do not. As such, the total contribution of the six central iron atoms should be decreased in an eight-iron model, as they make up a lesser fraction of the total iron intensity. The observed, diminished demand for the contributions of the two iron paths, therefore, is consistent with the expected fitting pat-

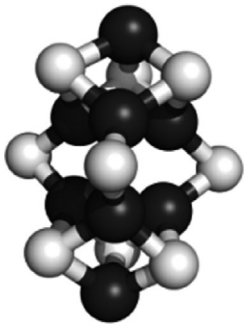

Figure 3. Structural model of isolated precursor. The eight-iron model of precursor was adapted from the crystallographic coordinates of the MoFe protein[12] but modified on the basis of the EXAFS fits. Fe black, S light gray.

tern of iron atoms in an eight-iron model. Second, when a single, approximately 2.7 Å iron path with a coordination number of 3.8 was included, the eight-iron model agreed poorly with the EXAFS data. However, if this path was split into two distinct paths—a 2.65 Å path with a coordination number of 3.3 and a 2.85 Å path with a coordination number of 0.5—the agreement of the eight-iron model to the EXAFS data was enhanced dramatically at a confidence interval of 0.98. A less dramatic effect was achieved at a confidence interval of 0.8 when a seven-iron model with coordination numbers of 3.1 and 0.3, respectively, for the 2.65 Å and 2.85 Å paths, was tested. The subsequent systematic exploration of the fitting space revealed that the quality of fit improved with an increase in the total iron coordination and, in particular, with higher coordination numbers for both distances. Taken together, both the final coordination numbers and the fitting behavior suggest the presence of not one, but two terminal iron atoms and, therefore, strongly favor the eight-iron model of the isolated precursor (see Supporting Information Tables S2 and S3 for the comparison of fit results of the six-, seven-, and eight-iron models, as well as the stepwise fitting procedure for the eight-iron model). This model is further supported by the outcome of the crystallographic analysis of NifEN, which reveals the presence of a nearly surface-exposed precursor in the protein that is compatible in geometry with an eight-iron analog of FeMoco.[9] Finally, it should be noted that the inclusion of backscattering from a lighter atom X (C, N, or O), which could originate from either a μ_6-interstitial atom[12] of the precursor or the solvent molecules, provided additional improvement to the fits (Table 4, Supporting Information S2 and S3).

In summary, the successful extraction of precursor from NifEN has permitted the first direct examination of its spectroscopic features without the interference of the $[Fe_4S_4]$ cluster. The integrity of the precursor is reflected by the restoration of the precursor-specific EPR signal, as well as the full proficiency of precursor in biosynthesis and catalysis upon its incorporation into Δ*nifB* NifEN. The observation that the precursor can readily reconstitute Δ*nifB* NifEN is in line with the presence of a complete cofactor core in the precursor structure, which is confirmed by the XAS/EXAFS analysis of the isolated precursor. An eight-iron model is defined for the isolated precursor, which suggests that the insertion of heterometal atom into the precursor during the maturation process of FeMoco involves the exchange of one of the terminal iron atoms for a molybdenum atom.

Received: April 19, 2011
Published online: July 1, 2011

Keywords: biosynthesis · FeMoco · nitrogenase · precursors · XAS/EXAFS

[1] B. K. Burgess, D. J. Lowe, *Chem. Rev.* **1996**, *96*, 2983 – 3012.
[2] Y. Hu, A. W. Fay, C. C. Lee, J. Yoshizawa, M. W. Ribbe, *Biochemistry* **2008**, *47*, 3973 – 3981.
[3] Y. Hu, J. M. Yoshizawa, A. W. Fay, C. C. Lee, J. A. Wiig, M. W. Ribbe, *Proc. Natl. Acad. Sci. USA* **2009**, *106*, 16962 – 16966.
[4] Y. Hu, A. W. Fay, M. W. Ribbe, *Proc. Natl. Acad. Sci. USA* **2005**, *102*, 3236 – 3241.
[5] M. C. Corbett, Y. Hu, A. W. Fay, M. W. Ribbe, B. Hedman, K. O. Hodgson, *Proc. Natl. Acad. Sci. USA* **2006**, *103*, 1238 – 1243.
[6] B. K. Burgess, *Chem. Rev.* **1990**, *90*, 1377 – 1406.
[7] The percentage of precursor incorporation was calculated from the spin quantitation (see Supporting Information) of the precursor-specific $S = 1/2$ signals of the reconstituted Δ*nifB* NifEN (Figure 1 a, experiment 3 minus experiment 2) and the as-isolated NifEN (Figure 1 a, experiment 4 minus experiment 2).
[8] J. M. Yoshizawa, M. A. Blank, A. W. Fay, C. C. Lee, J. A. Wiig, Y. Hu, K. O. Hodgson, B. Hedman, M. W. Ribbe, *J. Am. Chem. Soc.* **2009**, *131*, 9321 – 9325.
[9] J. T. Kaiser, Y. Hu, J. A. Wiig, D. C. Rees, M. W. Ribbe, *Science* **2011**, *331*, 91 – 94.
[10] A. W. Fay, M. A. Blank, J. M. Yoshizawa, C. C. Lee, J. A. Wiig, Y. Hu, K. O. Hodgson, B. Hedman, M. W. Ribbe, *Dalton Trans.* **2010**, *39*, 3124 – 3130.
[11] S. J. George, R. Y. Igarashi, Y. Xiao, J. A. Hernandez, M. Demuez, D. Zhao, Y. Yoda, P. W. Ludden, L. M. Rubio, S. P. Cramer, *J. Am. Chem. Soc.* **2008**, *130*, 5673 – 5680.
[12] O. Einsle, F. A. Tezcan, S. L. Andrade, B. Schmid, M. Yoshida, J. B. Howard, D. C. Rees, *Science* **2002**, *297*, 1696 – 1700.

